EEET ECOLOGICAL ENGINEERING & ENVIRONMENTAL TECHNOLOGY

Ecological Engineering & Environmental Technology 2024, 25(8), 297–307
https://doi.org/10.12912/27197050/190070
ISSN 2299–8993, License CC-BY 4.0

Received: 2024.06.10
Accepted: 2024.06.17
Published: 2024.07.01

Modification Graphite of Waste Batteries by Phosphotungstic Acid and Using as Photocatalyst for Methylene Blue Degradation

Wisam Abdalhusain Jabbar[1*], Marwa F. Abdul Jabbar[1]

[1] Al-Nahrain University, 1072 Baghdad, Iraq

* Corresponding author's e-mail: wissam.mche23@ced.nahrainuniv.edu.iq

ABSTRACT

In photocatalysis water treatments, Heteropoly acids impact is most used to realize effective separation of photo-generated carriers for active degrade organic pollutants. Here, a type of Heteropoly acids used as photocatalyst was prepared, (GHPT) consisted of phosphotungstic acid (PTA) with graphite prepared from a dry battery column and reactivated with hydrochloric acid (GH). Used assays (x-ray diffraction (XRD), fourier transform infrared spectroscopy (FTIR), field emission scanning electron microscopy (FESEM), BET surface area, energy dispersive x-ray (EDS) and element mapping images) were used to demonstrate the properties, composition, and components of the GHPT. To evaluate the catalytic activity of decomposition of methylene blue (MB) using LED light. The rate of MB decomposition can be affected by the type of catalyst, initial concentration of MB dye, removal time, catalyst dose, and pH. GHPT has many advantages for its practical application, through its properties as a photo-catalyst in terms of composition and components in the presence of light. The best removal percentage under the best conditions was 99.74 and total organic carbon analysis (TOC) percentage was 88.12 the at a concentration of 1 g/L of catalyst, an initial concentration of 25 ppm MB of MB, an illumination time of 180 minutes and a pH of 10.

Keywords: methylene blue, photocatalyst, graphite, phosphotungstic acid, deys.

INTRODUCTION

There has been a continuous increase in the growth of people in the world and the need for daily uses based on industry has led to an increase in human activities that have many influences on the biological society. Access to aquatic, both in goodness and amount, is one of the fundamental operators in determining the development of towns and metropolises as well as manufacturing (Ugya et al. 2019). On the other hand, it is the world's need to properly treat water for the purpose of reuse. The relationship of dyes to H_2O is generally complex because they hold their dye in the fibers during the textile manufacturing and under regular abrasion and tear with sunlight, aquatic and washing with detergents. Pigment is a soluble composite that can be absorbed or kept by fibers (Haddad et al. 2018). The paper manufacturing, rubber and plastic industrial, automobile process and textile manufacturing are the most widespread potential origins of pigment pollution in normal aquatic surfaces. Each year, approximately twelve millions persons miss their lives as a result of these waterborne sicknesses according to World Health Organization report 2011, and among these manufacturing, the textile manufacturing has taken the major role in environmental pollution, as it is accountable for soil and aquatic pollution (Newete et al. 2016). Manufactured dyes and derivatives are major carcinogenic and toxic pollutants (Saravanan et al. 2015).

Methylene blue (MB) is the substance frequently used in cotton dying, silk and wood. It can reason a burning sensation in the eye which may be accountable for enduring harm to the eyes of humanoid and faunas. When MB is inhaled, it can stretch growth to little times of fast or hard breathing while taken from the oral generates a scorching feeling and may reason

queasiness, cerebral confusion, puking, copious sweating and methemoglobinemia. Therefore, the process of effluent containing this color is important because of its damaging impacts on water (Rafatullah et al. 2010). Numerous technologies for treatment of dye manufacturing wastewater such as membrane filtration system, bio electrochemical removal, (Shindhal et al. 2021), advanced oxidation like the solar photo-Fenton (Foteinis et al. 2018), microbial treatment like Aspergillus carbonarius (Lakshmi et al. 2020) and photocatalysis removal like used ZnO Nanoparticles (Yerima et al. 2024 et al. 2024).Furthermore, solid waste spent batteries growth each year because more use of the portable electric equipment. Over eighty percent of batteries sold in European Union are a dry battery, the big plurality of dry batteries are alkaline and Zn-C batteries (Rahmawati et al. 2017). Nowadays, a large number of utilized batteries is disposed of, and this situation is considered the large environmental trouble for each country that stands in the way of developing electrics manufacturing (Le et al. 2022). Currently, with many premium features, like low poisonousness, moderate cost, easy spread in aquatic and more bioadaptability, carbon points have stimulated additional research in numerous fields, counting visual technique (sensor, diode discharge light), energy (catalytic, photovoltaics), and specially in biological implementation (fluorescence in body bioimaging, nanomedical) (Liu et al. 2020).

A photocatalyst is material that shows photocatalytic features, for example, the capability to promote and quicken specified chemical interactions when stimulated with light of convenient wavelength. Photocatalytic methods happen by the sharing of free electrons created in the photocatalyst over quantomechanical changeover of electrons into a moveable case by obliteration of the absorbed light particles. The nature of the free electrons is to spread over the surface of substance, until the redox interaction occurs between the reactants adsorbed on the area of the photocatalyst. thus, the "suitable" wavelength refers to wavelength that the photocatalyst absorbs well (Lettieri et al. 2021). A number of significant advantages for the nonhomogeneous photocatalysis have expanded their possible uses in H_2O Process, such as; (a) space working pressure and temperature, (b) complete mineralization of parents and their intermediates components is free from any side pollution and (c) the price of work is low (Chong et al. 2010).

Heteropoly acids are polyoxometalates (POMs) containing reactive mineral-O_2 clusters of the initial transition minerals (Vanadium, Niobium, Molybdenum, Tantalum, Tungsten) in their maximum oxidation case. Amongst polyoxometalates, Keggin-kind heteropoly anions composed of $[XM_{12}O_{40}]$ n- (X= hetero-atom as P5+, As5+, Si4+, Ge4+; M= Mineral as Mo6+, W6+, n = total cluster charge) keep most interest, in the first place due to their powerful Brønsted acidity quality, more thermic stability and trade obtainability (Sampurnam et al. 2019).

Phosphotungstic acid ($H_3PW_{12}O_{40}$) (PTA) is a good homogeneous photocatalytic, also is an electric acceptor or moderator for its good competence to receive or donate electrons with a well-defined Keggin form (Heng et al. 2016).

The idea of this research is to utilize a novel photocatalyst utilized in the LED-light process, which beat the conventional disadvantage of heterogeneous photocatalysts. In this research, new photocatalysts, PTA combined with waste Graphite from spent dry battery washed with Hydrochloric acid (HCL) to get photocatalytic (GHPT), the photocatalyst was prepared by mixing batch reactor process. Furthermore, due to its environmental prominence and non-biodegradation, methylene blue (MB) dye was chosen as a typical hydrocarbon to study the LED-light removal of dyes under the impact of GHPT.

MATERIALS AND METHODS

Materials

Phosphotungstic acid ($H_3PW_{12}O_{40}$) were purchased from Nanjing duly biotech co. ltd, China, Graphite from spent dry battery, Hydrochloric acid from Central Drag House (CDH) India, methylene blue ($C_{16}H_{18}CIN_3S$) from Merck, Germany, KOH from Sisco Research Laboratories Pvt. Ltd. India.

Preparation the graphite from the battery

First, the spent dry batteries are collected and the graphite rod is separated from the battery components (Bandi et al. 2019), The rod graphite is washed with 1 mol/L hydrochloric acid (HCL) solution for one hour (Bouleghlimat

et al. 2013), the purpose of HCL washing is to remove chemical components stuck to the graphite rod.

Mixing the solution at a speed of 300 rpm by Ceramic Magnetic Stirrer from Huanghua Faithful Instrument Co., Ltd/China, and the samples were cleaned with distilled water several times until the pH equal to 7(Al-Sairafi et al. 2022) dried for 5 hours at 100 °C , The purpose of drying for this time and temperature is to evaporate the water at a temperature of 100 °C and to ensure the elimination of excess moisture within the graphite voids, graphite (GH) is stored in a closed dry container for later use.

Preparation the phosphotungstic acid loaded on graphite (GHPT)

Prepared using the impregnation method (Wei et al. 2012), a certain amount of phosphotungstic acid (PTA) is used with GH in a loading ratio of (10%, 20%, 30%, 40%), the total weight of the two substances is 1 gram. The PTA is placed in a 150 ml beaker with 100 ml distilled water and mixed for 5 minutes on a flat magnetic stirrer at 300 rpm until it is completely dissolved. After that, GH is added so that the total weight is 1 gm and the Phosphotungstic acid to GH loading ratios are (10%, 20%, 30% and 40%), mix for an hour, then leave it overnight, place it in the oven for five hours and then store (GHPT) in a closed dry bottle until used later.

Description of the photocatalyst process for the batch reactor

Use an aluminum box measuring 65 × 35 × 52.5 cm. The light source radiates vertically onto the solution at a distance of 14 cm (Wang and Yang 2010). On one side of the box is placed a door that opens when samples are taken and closes tightly to prevent light from passing through it in the event of adsorption or during the photocatalytic process, 100 W LED lamps manufactured by Zhejiang AKKO STAR Electronic Technology Co., Ltd./China were used as a light exporter in the photocatalytic process. 100 ML of MB solution is placed in a 150 ml beaker on the magnetic stirrer at certain concentrations with 0.1 g of photocatalyst with a rotation speed of 300 rpm, the first 60 minutes is adsorption without light, then under the influence of LED light for 180 minutes. The process shown in Figure 1, over this operation, 2 ml of solution was taken every 30 minutes for each sample and analyzed using a UV-2900 spectrophotometer manufactured by Biotech Engineering Management Co. Ltd (UK), The photocatalytic removal efficiency percent (R%) was get as stated by the equation:

$$R\ (\%) = ((1 - (A/A_0)) \times 100 \quad (1)$$

RESULTS AND DISCUSSION

Morphological characteristics and textural properties

X-ray diffraction (XRD)

XRD patterns were determined on a Rigaku D-max C3 diffractometer using filtered Cu Kα radiation (1.5 = 1.541Å) to identify phases present in the decomposed samples. Figure 2 shows the XRD patterns of GH, GHPT (30 wt.%) compounds, The XRD pattern of GH which exhibits the diffraction peaks (2θ) at (20.7), (21.7), (24.1), (26.8), (42.8), (43.9), (44.4), (54.8), corresponds to (207.8), (778.0), (539.2), (5237.6), (283.4), (312.5), (312.5), (319.4), (77.9), (213.3) respectively. For GHPT, the peaks at (2θ) values

Figure 1. Photolysis process inside closed box

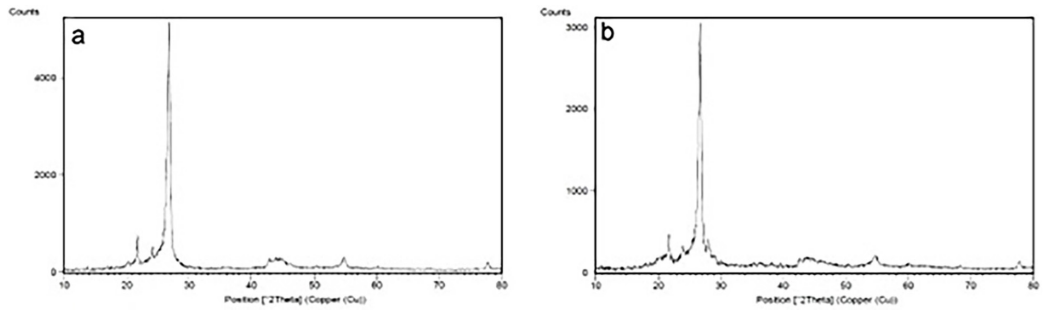

Figure 2. XRD patterns of (a) GH and (b) GHPT

of 21.7 (471.2), 24.0 (332.8), 26.7 (3115.7), 28.025 (418.7), 42.6 (178.6), 54.6 (210.9). The feature peaks became more apparent and sharpness upon PTA loading.

Fourier transform infrared spectroscopy (FT-IR)

Routine FT-IR spectrometer device manufactured by BRUKER AXS GmbH Germany Company was used to analyze the results of FTIR. Figure 3 illustrations the FTIR spectra of the three types catalysts. For graphite, the dominant peaks that are generally existing in graphitic material such as 1066.5, 1395, 2061, 2170, 2790 and 2988 cm^{-1} agree to the stretching of C-O, asymmetric dilation vibration of C-H, and dilation of C=C. The broad peak linked to the vibration of the hydroxyl (–OH) group also can be seen at a wavenumber up 3500 cm^{-1} (Destiarti and Sasri 2020). Four fundamental FITR bands features of the Keggin form can be seen well for fresh PTA: 1072.42, 973.05, 903.35, 775.27 cm^{-1}, imputed to (P–O_a), (W–O_t), (W–O_b–W) and (W–O_c–W) vibrations correspondingly. These bands are linked to changed kinds of O_2 in the Keggin form: O_2 of the central tetrahedral phosphate (O_a), the terminal O_2 linked to tungsten atom single (O_t), the bridge O_2 amidst two various W_3O_{13} groups (O_b) and the bridge O_2 in the similar W_3O_{13} group O_2 corner (O_c) and the conformable peaks can be located in GHPT (Lopes da Costa et al. 2021). The feature peak of PTA has a little deviation, which can be explained by the fact that only couple of electrons in the organic positive ion spreads into the inorganic structure of the POMs negative ion, which gives the creation of a powerful electric force amid the two so that the features of together edges and the absorption peaks are somewhat changed (Zheng et al. 2022).

Field emission scanning electron microscopy (FESEM)

The morphological characteristics of the surface components of GH and GHPT were determined by FE-SEM analyzes (SEM testing machine called VEGA III, TESCAN). Figure 4a, the pores of the graphite appear clearly, while Figure 4b shows the distribution of PTA loaded on the graphite surface, where the distribution is in two forms. The first is similar to a dotted distribution on the graphite surface, and the second form shows an agglomeration extending over the surface area of PTA on the graphite surface. Figure 5 shows the element mapping images for GH and GHPT, the images shows that elements C, N, O, components of PTA groups, represented by P, W, and O elements, are well dispersed in the C-element arrays of GH. It strongly confirms the highly dispersed PTA clusters on the GH surface in their heterogeneous photocatalyst.

BET surface area and average pore diameter (PD)

As for the, there was an increase after adding PTA from 6.38 (m^2 g^{-1}) to 16.44 (m^2 g^{-1}), The opposite of what happens in PD, where PD decreases after loading PTA from 4.9282 nm to 2.998 nm. The specific surface area and average pore diameter was scaled by the BET-BJH system using N2 adsorption and desorption tests employing Micromeritics ASAP 2010.

Energy dispersive X-Ray (EDS)

EDS analysis was used to reveal the existence of genuine elements in both GH and GHPT samples. For the GH spectrum as shown in Figure 6a, a high peak is observed at 0.285 keV matching to the spectral line K of GH. For GHPT, Figure 6b displays two clear peaks at approximately 1.41 and 1.78 keV (line M) and (line L) five 7.37, 8.41, 9.68, 9.97 and 11.31 keV indicating the tungsten

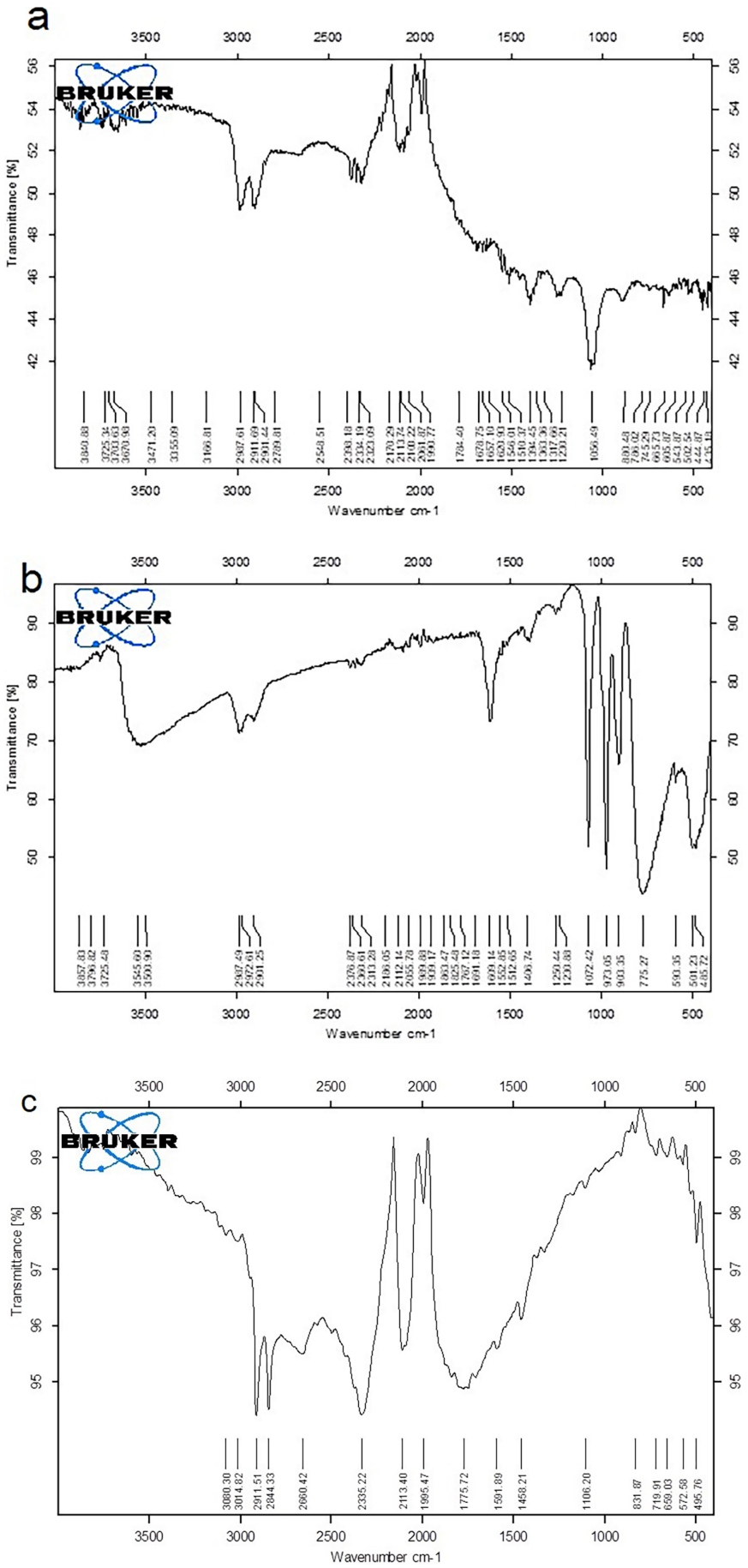

Figure 3. FTIR of (a) GH, (b) PTA, (c) GHPT

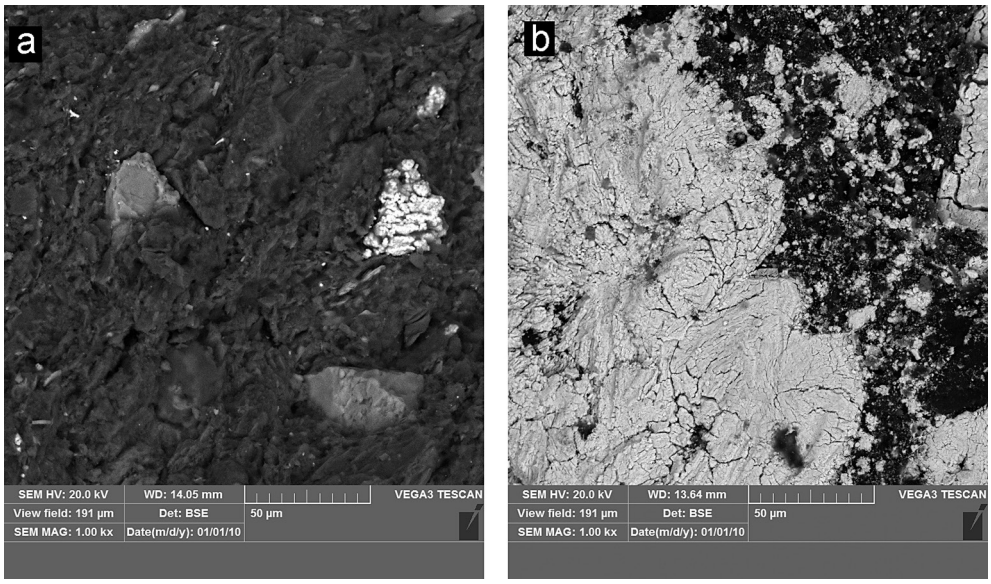

Figure 4. SEM images of (a) GH and (b) GHPT

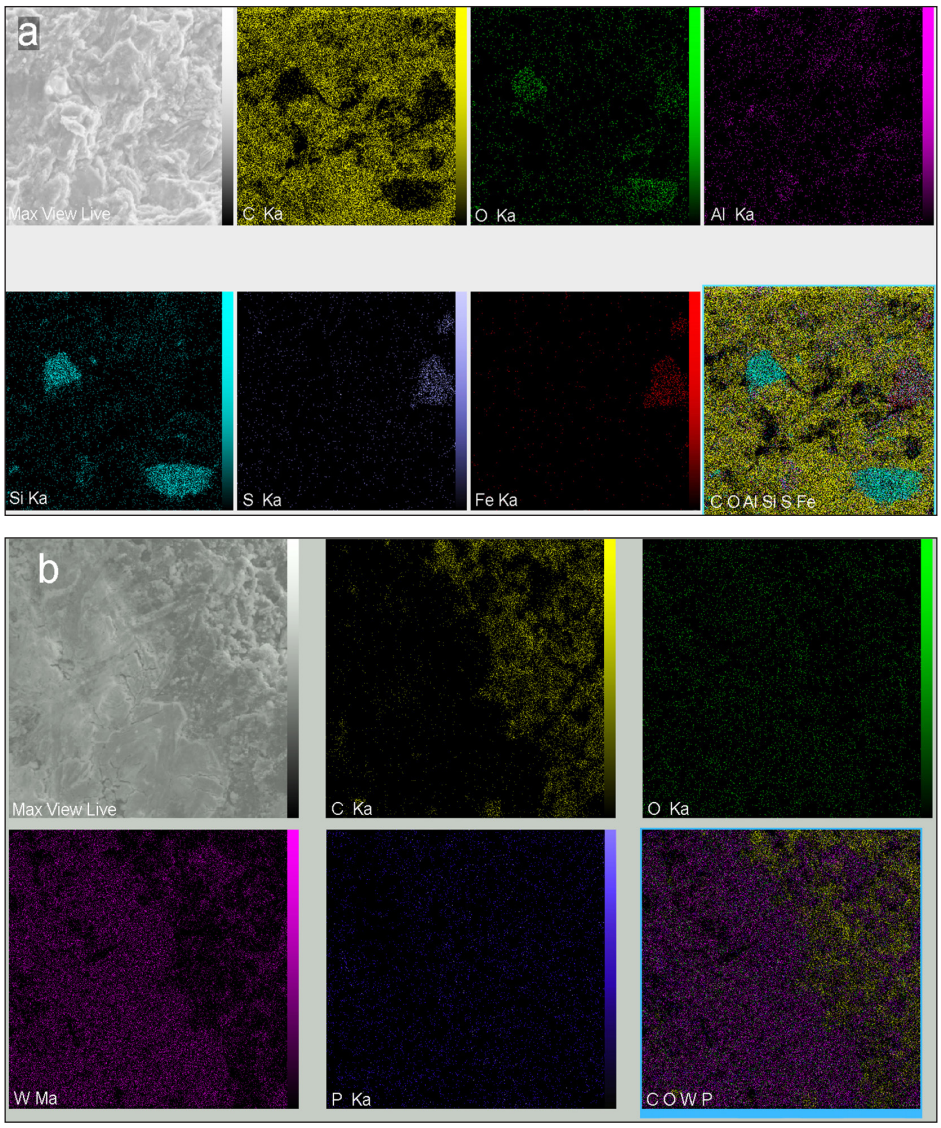

Figure 5. The element mapping images of (a) GH, (b) GHPT

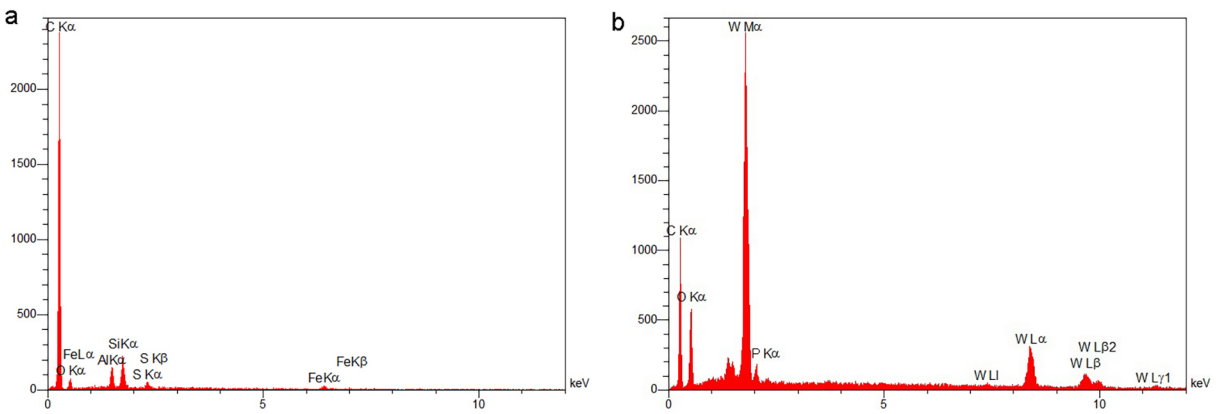

Figure 6. EDS of (a) GH and (b) GHPT

atom (W), At (line K) the atoms (C), (O) and (P) appear at 0.28, 0.53 and 2.03 keV respectively. EDX profiles are shown after loading PTA onto GH and after dissolution tests. The atoms formed in the form of PTA match the spectral lines of the composite compounds of GHPT, which indicates the excellent stability of the materials loaded on the surface of GH, in addition to atoms (O, Fe, Al, Si, S) with low peak levels.

Parameters effect on the removal percent of MB

Effect of GHPT amount

The effect of catalyst dose of GHPT (0.25, 0.5, 1, 2 g/L) on the removal percent is shown in Figure 7. The results presented that the photodegradation rate of MB raised from 38.75%, to 47.29% when the photocatalyst dose was raised from (0.25 to 0.1 g/L) respectively during 180 minutes of LED light. The catalyst dose at 2 g/L requires half the photolysis time compared to the dose of 0.25 g/L at 180 minutes. However, when the dose was 2 g/L, the highest photodegradation value within 180 minutes reached 54.32%.

Effect of pH solution

Figure 8 shows the effect of PH solution on the removal percent of MB dye (2, 3, 5, 7, 10 and 12), conditions of experimental (initial concentration 25 ppm, dose of GHPT 1 g/L, loading percent 30% PTA). At pH 2, after 180 minutes, the

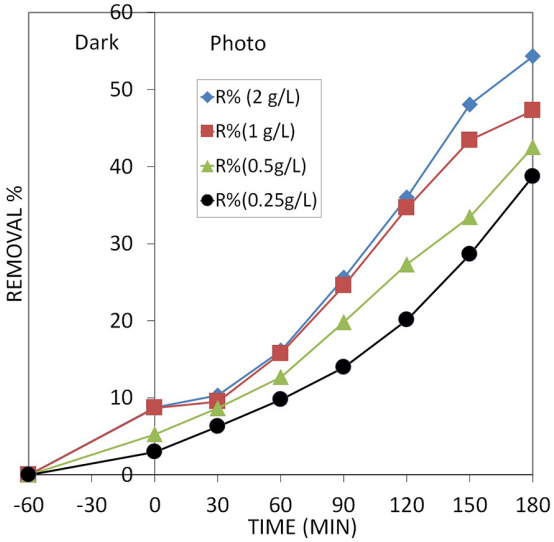

Figure 7. The effect of catalyst dose of GHPT on the removal percent of MB dye, conditions of experimental (Initial concentration 25 ppm, pH=5, loading percent 30% PTA)

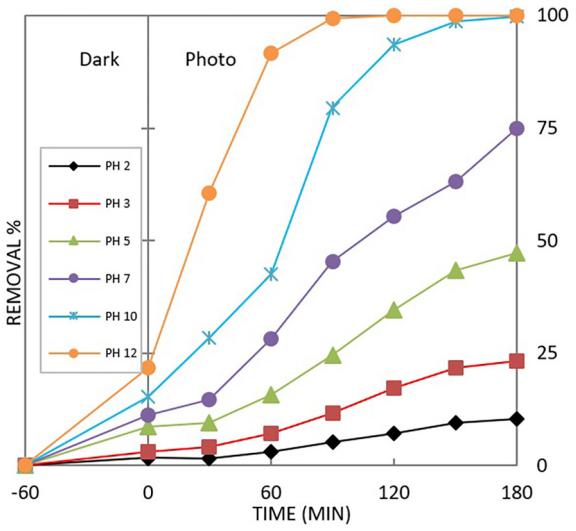

Figure 8. The effect of solution pH on the Removal percent of MB dye (2,3,5,7,10 and 12), conditions of experimental (Initial concentration 25 ppm, Dose of GHPT 1 g/L, loading percent 30% PTA

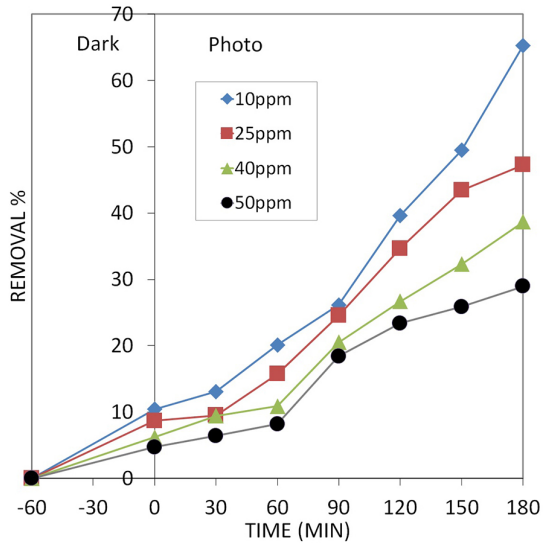

Figure 9. The effect Initial concentration of solution MB (10,25,40 and 50) on the removal percent of MB dye, conditions of experimental (Dose of GHPT 1 g/L, loading percent 30% PTA, pH = 5)

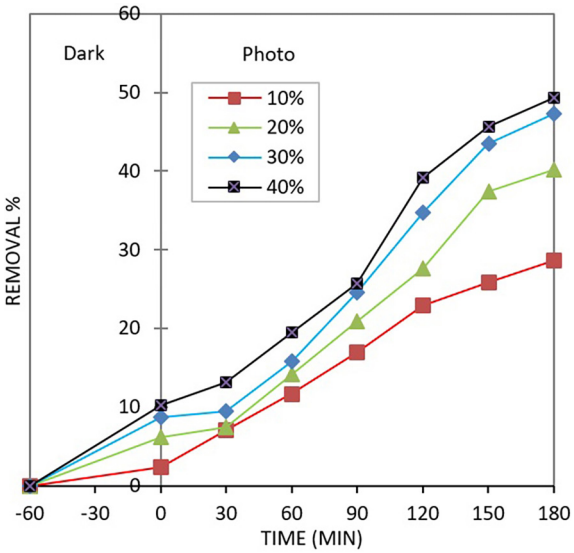

Figure 10. The Effect loading percent of PTA on GH (10, 20, 30 and 40%) on the removal percent of MB dye, conditions of experimental (Initial concentration 25 ppm, Dose of GHPT 1 g/L, pH = 5)

removal percentage is small and only 10%, and at pH 3 the removal percentage reaches 23% at the same time. At pH 5, removal is approximately twice that of pH 3, removal is three-quarters complete at pH 7 to reach 74.91%, and at pH 10 removal is almost complete at 180 min. While in Ph12 in just 120 minutes.

Effect of initial MB concentration

Figure 9 illustrations the effect of solution MB initial concentration on the degradation of MB dye. Increasing the concentration of the dye is inversely proportional to the photodegradation rate. At a concentration of 50 ppm, the removal rate reaches 28.95%, then it increases at a cumulative rate of 10% at each concentration (40 and 25) ppm, respectively, and reaches the highest photodegradation rate of 65.30% at 10 ppm.

The effect loading percent of phosphotungstic acid on graphite

Figure 10 shows the effect loading percent of PTA on GH (10,20,30 and 40%) on the removal percent of MB dye, conditions of experimental (initial concentration 25 ppm, dose of GHPT 1 g/L, pH = 5). The removal percentage increases with the PTA loading percentage, as at the loading percentages (10, 20, 30, and 40), the removal percentages are 28.59, 40.12, 47.29, and 49.33, respectively.

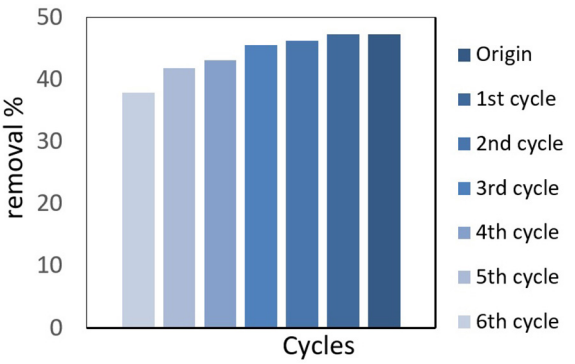

Figure 11. Recyclability of GHPT

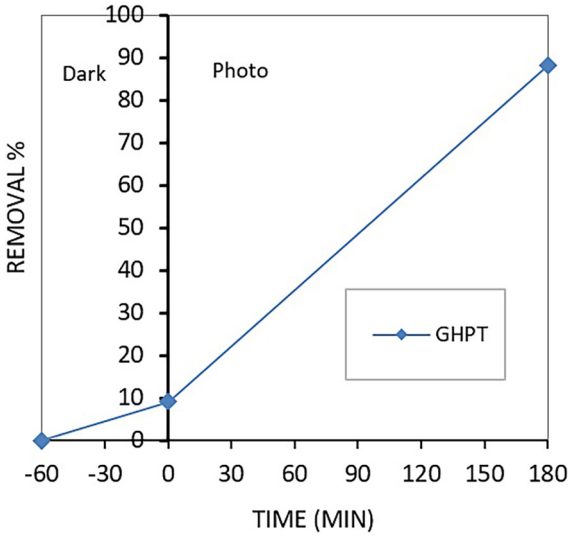

Figure 12. TOC of GHPT at dose 1 g/L, a pH 10, Initial concentration: 25 ppm of MB

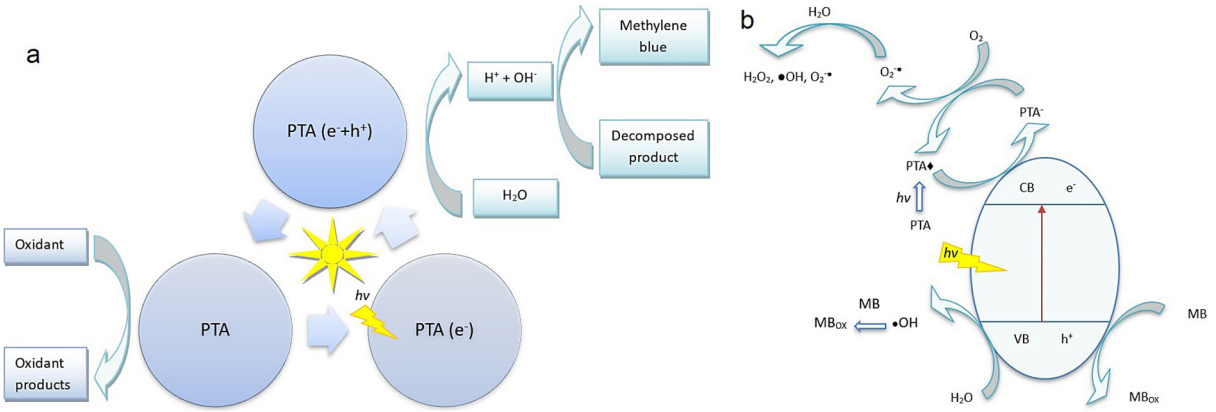

Figure 13. (a) Mechanism of removing methylene blue using GHPT photocatalysis and (b) Detailed mechanism of transfer of photogenerated electrons by GHPT in the presence of light

Recyclability

To prove the photocatalytic persistence and reusability for many times, GHPT was tested six times for the removal of MB at the same conditions. Figure 11 shows the removal efficiency for 6 cycles. It was noted that the removal rate decreased by a few percentages after each cycle. The removal rate in the first cycle reached 47.25%, while the removal rate in the sixth cycle was 37.92%, and this indicates that the graphite retained high percentages of PTA, which causes photocatalysis.

Total organic carbon analysis (TOC)

Total organic carbon (TOC) is the scale of the mass of carbon obtainable in an organic composite and is frequently utilized as a primary agent for unconventional shale resource appraisal (Mahmoud et al. 2017). TOC at a pH of 10 was also used to determine the best removal percentage that could be achieved under the conditions of 25 ppm of MB, dose of GHPT 1 g/L and an illumination time of 180 minutes, where the percentage reached 88.12 compared to adsorption for 60 minutes, the percentage was 9.09. As shown in Figure 12.

Activity of photocatalyst in degradation

In order to determine the catalyst effectiveness of GHPT utilized as a photocatalytic process, comparative tests were performed under various conditions. As shown in Table 1, the decomposition percentage at 180 min with darkness for GHPT was 8.68%. However, the degradation percentage reached 47.92% and 42.18% respectively using the LED light process. Obviously,

Table 1. A comparison between the action of photocatalysts in the presence and absence of light. Experimental conditions: dose of photocatalyst 0.1 g, 100 mL MB solution, pH = 5, initial concentration of MB solution 25 ppm

The state of catalyst	Removal %
GHPT in dark	8.68
GHPT in LED Light	47.92
GH in LED Light	23.43

the action of GHPT can efficiently catalyze the creation of •OH with LED light process.

Furthermore, in the absence of the removal ratio of MB is 23.43% with GH and LED light, which confirms the generation of •OH under the action of GHPT under LED light. On the base of empirical analysis, the reaction mechanism of the photocatalyst system can be explained by the following reactions:

$$PTA + h\nu. \rightarrow PTA* \quad (2)$$

$$PTA* + H2O \rightarrow PTA^{-} + {}^{\cdot}OH + H^{+}\,b \quad (3)$$

$$MB + {}^{\cdot}OH^{-} \rightarrow \text{Degradations} \quad (4)$$

where: PTA^{-} denotes the $H_3PW_{12}O_{40}$ respectively in reducing case (Wei et al. 2012).

Mechanism

PTA have a semiconductor-similar electronic form, which consists of an electron-occupied valence band (VB) and a void conduction band (CB). Generally, as apparent in Figure 13a when the PTA is affected by radiant energy, it leads to work action parallel to or more than its band gap, the electrons in the VB are mobile to the CB, performing

in photoproduced electrons (e−) and holes (h+). h+ are than generate ●OH with methylene blue in the existence of H_2O. ●OH, have intense oxidizing charlatanistic which are used as efficient atoms for the oxidation and removal methylene blue Figure 13b PTA collect photocreated electrons from the GH surface and forms a PTA− atoms by decreasing. This process retards the reassemble of h+ and e− couples and gives the generation of ●OH by h+ great effective. Temporarily, PTA− atoms moves an electron to the dissolved O_2 in the mixture to produce oxygen radicals O_2−● , it then reacts with H_2O to yield ●OH and/or H_2O_2 species, further oxidizing methylene blue (Lan et al. 2021).

CONCLUSIONS

Through XRD and FTIR analyses, the GHPT photocatalyst demonstrated good loading results of Phosphotungstic acid, as PTA peaks on the GH surface were detected through comparison between tests before and after loading. A large amount of PTA was seen in the photocatalyst by SEM images, the components of the Keggin formula were clearly visible in the MAPPING images and EDS results as well as the increased surface area of the photocatalyst compared to GH. The MB was almost completely decomposed under LED lamp with GHPT, and the result showed that the removal percentage was up to 99.74 and the TOC percentage was 88.12 at a dose of 1 g/L of catalyst, an initial concentration of 25 ppm of MB, an illumination time of 180 minutes and a pH of 10. The study concluded that this type of catalyst has great potential for photo-oxidized organic dye wastewater treatment at basic levels due to the formation of hydroxyl radicals.

REFERENCES

1. Al-Sairafi F.A., Jiang C., Zhong Z., Saleh B. 2022. Study on Purification of Flake Graphite by Heat Activation and Hydrofluoric Acid. Advances in Materials and Processing Technologies, 8(4), 4564–78. https://doi.org/10.1080/2374068X.2022.2079172
2. Bandi S., Ravuri S., Peshwe D.R., Srivastav A.K. 2019. Graphene from Discharged Dry Cell Battery Electrodes. Journal of Hazardous Materials, 366, 358–69. https://doi.org/10.1016/j.jhazmat.2018.12.005
3. Bouleghlimat E., Davies P.R., Davies R.J., Howarth R., Kulhavy J., Morgan D.J. 2013. The effect of acid treatment on the surface chemistry and topography of graphite. Carbon, 61, 124–33. https://doi.org/10.1016/j.carbon.2013.04.076
4. Chong M.N., Jin B., Chow C.W.K., Saint C. 2010. Recent developments in photocatalytic water treatment technology: A review. Water Research, 44(10), 2997–3027. https://doi.org/10.1016/j.watres.2010.02.039
5. Destiarti L., Sasri R. 2020. Application of titanium-silica-graphite composite material for photocatalytic process of methylene blue. Indonesian Journal of Chemistry, 20(6), 1271–82. https://doi.org/10.22146/ijc.48998 .
6. Foteinis S., Monteagudo J.M., Durán A., Chatzisymeon E. 2018. Environmental sustainability of the solar photo-fenton process for wastewater treatment and pharmaceuticals mineralization at semi-industrial scale. Science of the Total Environment, 612, 605–12. https://doi.org/10.1016/j.scitotenv.2017.08.277
7. Haddad M., Abid S., Hamdi M., Bouallagui H. 2018. Reduction of adsorbed dyes content in the discharged sludge coming from an industrial textile wastewater treatment plant using aerobic activated sludge process. Journal of Environmental Management, 223, 936–46. https://doi.org/10.1016/j.jenvman.2018.07.009.
8. Heng H., Gan Q., Meng P., Liu X. 2016. H3PW12O40/TiO2-In2O3: A visible light driven type-ii heterojunction photocatalyst for the photocatalytic degradation of imidacloprid. RSC Advances, 6(77), 73301–7. https://doi.org/10.1039/c6ra10729j
9. Lakshmi S., Suvedha K., Sruthi R., Lavanya J., Varjani S., Nakkeeran E. 2020. Hexavalent chromium sequestration from electronic waste by biomass of Aspergillus carbonarius. Bioengineered, 11(1), 708–17. https://doi.org/10.1080/21655979.2020.1780828
10. Lan J., Wang Y., Huang B., Xiao Z., Wu P. 2021. Application of polyoxometalates in photocatalytic degradation of organic pollutants. Nanoscale Advances, 3(16), 4646–58. https://doi.org/10.1039/d1na00408e
11. Le P.A., Le V.Q., Nguyen N.T., Nguyen V.T., Thanh D.V., Phung T.V.B. 2022. Multifunctional applications for waste zinc-carbon battery to synthesize carbon dots and symmetrical solid-state supercapacitors. RSC Advances, 12(17), 10608–18. https://doi.org/10.1039/d2ra00978a
12. Lettieri S., Pavone M., Fioravanti A., Amato L.S., Maddalena P. 2021. Charge carrier processes and optical properties in TiO2 and tio2-based heterojunction photocatalysts: a review. Materials, 14 (7). https://doi.org/10.3390/ma14071645
13. Liu Y., Hui H., Cao W., Mao B., Liu Y., Kang Z. 2020. Advances in carbon dots: from the perspective of traditional quantum dots. Materials Chemistry Frontiers, 4(6), 1586–1613. https://doi.org/10.1039/d0qm00090f

14. Lopes da Costa N., Pereira L.G., Resende J.V.M., Mendoza C.A.D., Ferreira K.K., Detoni C., Souza M.M.V.M., Gomes F.N.D.C. 2021. Phosphotungstic Acid on Activated Carbon: A Remarkable Catalyst for 5-Hydroxymethylfurfural Production." Molecular Catalysis 500 (August 2020). https://doi.org/10.1016/j.mcat.2020.111334
15. Mahmoud A., Elkatatny S., Mahmoud M., Abouelresh M., Abdulraheem A., Ali A. 2017. Determination of the Total Organic Carbon (TOC) Based on Conventional Well Logs Using Artificial Neural Network. International Journal of Coal Geology, 179, 72–80. https://doi.org/10.1016/j.coal.2017.05.012
16. Newete S.W., Erasmus B.F.N., Weiersbye I.M., Byrne M.J. 2016. sequestration of precious and pollutant metals in biomass of cultured water hyacinth (Eichhornia Crassipes). Environmental Science and Pollution Research, 23(20), 20805–18. https://doi.org/10.1007/s11356-016-7292-y
17. Rafatullah M., Sulaiman O., Hashim R., Ahmad A. 2010. Adsorption of methylene blue on low-cost adsorbents: a review. Journal of Hazardous Materials, 177(1–3), 70–80. https://doi.org/10.1016/j.jhazmat.2009.12.047
18. Rahmawati F., Leny Yuliati L., Alaih I.S., Putri F.R. 2017. Carbon rod of zinc-carbon primary battery waste as a substrate for CdS and tio2 photocatalyst layer for visible light driven photocatalytic hydrogen production. Journal of Environmental Chemical Engineering, 5(3), 2251–58. https://doi.org/10.1016/j.jece.2017.04.032
19. Sampurnam S., Muthamizh S., Dhanasekaran T., Latha D., Padmanaban A., Selvam P., Stephen A., Narayanan V. 2019. Synthesis and characterization of keggin-type polyoxometalate/zirconia nanocomposites—comparison of its photocatalytic activity towards various organic pollutants. Journal of Photochemistry and Photobiology A: Chemistry, 370, 26–40. https://doi.org/10.1016/j.jphotochem.2018.10.03
20. Saravanan R., Gupta V.K., Mosquera E., Gracia F., Narayanan V., Stephen A. 2015. Visible light induced degradation of methyl orange using β-Ag0.333V2O5 nanorod catalysts by facile thermal decomposition method. Journal of Saudi Chemical Society, 19(5), 521–27. https://doi.org/10.1016/j.jscs.2015.06.001
21. Shindhal T., Rakholiya P., Varjani S., Pandey A., Ngo H.H., Guo W., Ng H.Y., Taherzadeh M.J. 2021. A critical review on advances in the practices and perspectives for the treatment of dye industry wastewater. Bioengineered, 12(1) 70–87. https://doi.org/10.1080/21655979.2020.1863034
22. Ugya A.Y., Hua X., Ma J. 2019. Phytoremediation as a tool for the remediation of wastewater resulting from dyeing activities. Applied Ecology and Environmental Research, 17(2), 3723–35. https://doi.org/10.15666/aeer/1702_37233735
23. Wang W., Yang S. 2010. Photocatalytic degradation of organic dye methyl orange with phosphotungstic acid. Journal of Water Resource and Protection, 2(11), 979–83. https://doi.org/10.4236/jwarp.2010.211116
24. We G., Zhang L., Wei T., Luo Q., Tong Z. 2012. "UV-H2O2 degradation of methyl orange catalysed by H3PW12O40/activated clay. Environmental Technology (United Kingdom), 33(14), 1589–95. https://doi.org/10.1080/09593330.2011.639395
25. Yerima E.A., Ogwuche E., Ndubueze C.I., Muhammed K.A., Habila J.D. 2024. Photocatalytic degradation of acid blue 25 dye in wastewater by zinc oxide nanoparticles. Trends in Ecological and Indoor Environmental Engineering, 2(1), 50–55. https://doi.org/10.62622/teiee.024.2.1.50-55
26. Zheng M., He H., Li X., Yin D. 2022. Imidazolized activated carbon anchoring phosphotungstic acid as a recyclable catalyst for oxidation of alcohols with aqueous hydrogen peroxide. Frontiers in Chemistry, 10, 1–13. https://doi.org/10.3389/fchem.2022.925622